

Solvent-Engineered Scalable Production of Polysulfide-Blocking Shields to Enhance Practical Lithium–Sulfur Batteries

Jin-Lei Qin, Hong-Jie Peng, Jia-Qi Huang,* Xue-Qiang Zhang, Long Kong, Jin Xie, Meng Zhao, Ruiping Liu*, Huiyou Zhao, and Qiang Zhang*

Lithium–sulfur (Li–S) batteries are very promising next-generation energy-storage devices due to the extremely high energy density. However, the low capacity and poor cycling life induced by the shuttle effect of polysulfide intermediates impede the practical application of Li–S batteries. Here, a very effective solvent-engineering strategy is proposed to fabricate thin, compact, and multifunctional binary solvent–engineered polysulfide-blocking shields (BBSs) with a superior capability of retarding the shuttle and stabilizing the cathode/anode. The Li–S batteries with a BBS separator exhibit enhanced cell kinetics, superb cycling stability with a low decay rate of 0.078% per cycle for 400 cycles at 0.5 C, and a high areal capacity of 4.91 mAh cm^{−2} after 100 cycles at 2.37 mA cm^{−2}. In addition, the industrially viable fabrication of BBS is readily employed in practical Li–S pouch cells. The concept of solvent engineering not only renders functional interlayers/separators that significantly improve the Li–S battery performance but also is simple, versatile, and scalable to be adopted for many other promising research fields of energy storage and materials chemistry.

lithium–sulfur (Li–S) batteries provide a promising option that could theoretically achieve the highest gravimetric specific energy of 2600 Wh kg^{−1} at a practically low cost. The huge advantage in theoretical energy density over current lithium-ion batteries is promised by the exploration of high-capacity rechargeable lithium metal anodes and sulfur cathodes.^[2] The unique Li–S chemistry in commonly employed aprotic electrolytes, however, induces a dominant phenomenon, namely the so-called “shuttle” effect: a series of soluble intermediates, lithium polysulfides (Li₂S_x, 2 < x ≤ 8, denoted as LiPSs), are generated during discharge and diffuse between the cathode and anode under the driving forces of concentration gradient and electric fields, inducing the internal consumption of active materials, lowering the energy efficiency, and degrading the cell rechargeability and cyclability.^[3,4]

Alkali metal (Li/Na/K)–chalcogen (S/Se) batteries emerge as an ensemble of next-generation secondary battery systems to meet the requirements from rapidly expanding markets of energy storage and power sources.^[1] Among them,


Along with the intrinsic low electronic/ionic conductivity of sulfur/lithium (di)sulfide (Li₂S₂/Li₂S), the shuttle effect strongly impedes the development of practically viable Li–S batteries with high capacity, high efficiency, high cyclability, and high safety. Thus, one of the kernels in developing practical Li–S batteries is mitigating the shuttle effect.

Inserting a conductive interlayer between the cathode and the separator or alternatively coating the routine porous separator with a functional layer is recognized as an efficient and effective strategy to mitigate the shuttle effect.^[5] As first proposed by Su and Manthiram,^[6] such a conductive and porous (inter)layer can not only retard the crossover of LiPSs through steric confinement but also reutilize the LiPSs escaping from the cathode. Various carbonaceous materials such as carbon blacks, carbon nanotubes (CNTs), graphene, and porous carbons have been employed to build a functional (inter)layer.^[7–9] Hydrophilic polymers and inorganic metal compounds could further functionalize this layer with favorable chemical affinities to enhance the immobilization of LiPSs.^[10–14] The above progresses in separator/interlayer design all exhibit certain benefits to improve Li–S batteries. Nevertheless, this strategy is always questioned because it introduces extra weight and volume, which may offset the performance enhancement at a device scale. Besides, previously reported fabrication methods

J.-L. Qin, Prof. R. P. Liu, Prof. H. Y. Zhao
Department of Materials Science and Engineering
China University of Mining and Technology (Beijing)
Beijing 100083, China
E-mail: lrp@cumt.edu.cn

J.-L. Qin, H.-J. Peng, X.-Q. Zhang, Dr. L. Kong, J. Xie, Prof. Q. Zhang
Beijing Key Laboratory of Green Chemical Reaction Engineering and Technology
Department of Chemical Engineering
Tsinghua University
Beijing 100084, China
E-mail: zhang-qiang@mails.tsinghua.edu.cn

Prof. J.-Q. Huang, M. Zhao
Advanced Research Institute of Multidisciplinary Science
Beijing Institute of Technology
Beijing 100081, China
E-mail: jqhuang@bit.edu.cn

 The ORCID identification number(s) for the author(s) of this article can be found under <https://doi.org/10.1002/smt.201800100>.

DOI: 10.1002/smt.201800100

in many cases are feasible in laboratory but hardly practicable for large-scale industrial applications (e.g., vacuum filtration). Therefore, it is important for a functional interlayer or coating layer applied in Li–S batteries 1) to reduce its weight and thickness, 2) to be fabricated in a practically preferred manner, and 3) to achieve superior shuttle suppression in practical cell with high sulfur loading.

Up to now, there have been several prototype ultrathin functional interlayers or coating layers reported for Li–S batteries, including shear-aligned nematic graphene oxide (GO) membrane (0.75 μm),^[15] GO-supported Nafion membrane (0.15 μm),^[16] and naphthalimide-functionalized poly(amidoamine) dendrimer/GO composite film (0.1 μm).^[14] Nevertheless, it is still challenging to scale up the fabrication of the above ultrathin layers due to either the involvement of vacuum filtration or the employment of unready on-shelf materials like nematic GO. Recently, Yang and co-workers presented a facile electrostatic spraying to generate an ultrathin and compact coating (0.1 μm) on the sulfur cathode,^[17] indicating that besides innovations in material itself, advances in material processing that is simple, green, and scalable may create new opportunities for efficient usage of new material.

In this contribution, we propose a very simple solvent-engineering strategy by replacing the conventional single-solvent slurry to a binary-solvent slurry in industrially compatible blade-coating production. Through this strategy, large pieces of thin, compact, and multifunctional LiPS-blocking shield can be continuously fabricated, allowing rapid solvent drying at a mild temperature and requiring no extra time-/energy-consuming steps such as calendaring. Such a binary solvent-engineered LiPS-blocking shield (BBS, in against to single-solvent-engineered polysulfide-blocking shield (SBS) prepared from a single-solvent slurry) consists of hydrophilic polymer matrix to chemically trap LiPSs and a highly conductive carbon skeleton to reutilize the trapped sulfur species. Consequently, both the sulfur cathode and the lithium anode can be effectively stabilized in working Li–S cells equipped with a BBS separator, leading to enhanced rate and cycling performance. More importantly, the lightweight and thin BBS also works well in practically favorable high-sulfur-loading Li–S coin and pouch cells without sacrificing the device weight and volume.

This strategy is inspired from the basic physical chemistry of colloid assembly. In fact, the film formation from precursor slurry resembles the solvent evaporation-induced assembly of colloid nanocrystals into superlattice, which is one of the most extensively employed methodologies for superlattice assembly.^[18] However, it always takes a long duration to obtain an ideal and compact film (superlattice) as a delicate equilibrium in colloid–solvent–substrate is usually required. In this case, colloidal particles wrapped by polymer binder (ligands) are initially well stabilized in a good solvent, which has high solubility of polymer (ligands) so to induce considerable interparticle repulsion through solvent osmosis (Figure 1a). The strong repulsion forces prevent the effective clustering of colloidal particles until the very late stage of solvent drying, at which the particle volume fraction increases to the threshold of precipitation. If there is an obvious difference in polarity between the solvent and the deposition substrate, the colloid solution with a low solvent volume fraction will be prone to form isolated

droplets, driven by strong surface tension (Figure 1b). Further drying consequently results in a nonuniform and defective film (colloidal aggregation) of SBS and LiPSs can easily diffuse through the cracks and defects, inducing a controlled shuttle effect (Figure 1c). Therefore, simple solvent evaporation cannot synchronously meet the requirements of high time efficiency and good film (superlattice) quality.

In this regard, the concept of another methodology for superlattice assembly, i.e., solvent destabilization, is introduced herein. The basic idea of solvent destabilization is to introduce a poor solvent for polymer (ligands) to the precursor slurry (nanocrystal solution).^[18] According to the Flory–Krigbaum theory,^[19] the lowered solvent quality, i.e., poor solubility of polymer (ligands), weakens the osmosis-induced interparticle repulsion (Figure 1d). Thus, the polymer-wrapped (ligand-protected) colloidal particles can be attracted and diffuse to form clusters prior to the late stage of solvent drying, at which the threshold of particle volume fraction for precipitation is also higher owing to the lower solubility of binary solvent than the single good one. The solvent evaporation thus will leave a more compact and spread solution film on the substrate if the polarity difference between the substrate and the good solvent is smoothed out by introducing another solvent with an opposite polarity (Figure 1e). After complete drying, a compact film of BBS can be expected with superior steric and chemical shielding effect on LiPS diffusion (Figure 1f). The reduced interparticle repulsion, correspondingly enhanced attraction, contributes to achieve a thin coating.

To prove the above solvent-engineering concept, highly conductive graphene/carbon nanotube (G/CNT) hybrids and hydrophilic polyacrylic acid (PAA)-based binder were selected as the building blocks to endow the as-fabricated BBS with multifunctionalities including 1) desirable chemical affinity of carboxylic-rich PAA binder to LiPSs,^[11] 2) high electrical conductivity of G/CNT hybrids to reutilize the trapped LiPSs, and 3) hierarchical porosity to enable facile ion transport and to strengthen the mechanical properties. The G/CNT hybrid has previously been demonstrated to be produced continuously at a large quantity using a fluid-bed chemical vapor deposition technology and now is a successfully industrialized nanomaterial.^[20] The commercial available G/CNT hybrids are featured with porous graphene sheets interlinked by few-walled CNTs (Figure S1, Supporting Information). This structural characteristic has shown its advantages in preventing the restacking of graphene sheets and agglomeration of CNTs, benefiting a good electrochemical performance of Li–S batteries in earlier studies.^[21] The G/CNT hybrid employed herein has an extremely high surface area of 2132 $\text{m}^2 \text{g}^{-1}$, a large pore volume of 3.27 $\text{cm}^3 \text{g}^{-1}$ (for pores with a size of <30 nm), and abundant mesopores to effectively accommodate and reutilize a large amount of sulfur species (Figure S2, Supporting Information). PAA is a typical commercial aqueous binder, allowing to use safe, green, and nontoxic solvent of water. Therefore, both the two building blocks are readily on-shelf products for bulk applications.

Water as a solvent has many advantages for industrial production and applications. Nevertheless, water is a too good solvent for PAA and possesses large surface tension, thereby unfortunately dropping in the dilemma described in Figure 1a–c. To shift the paradigm from single solvent to binary

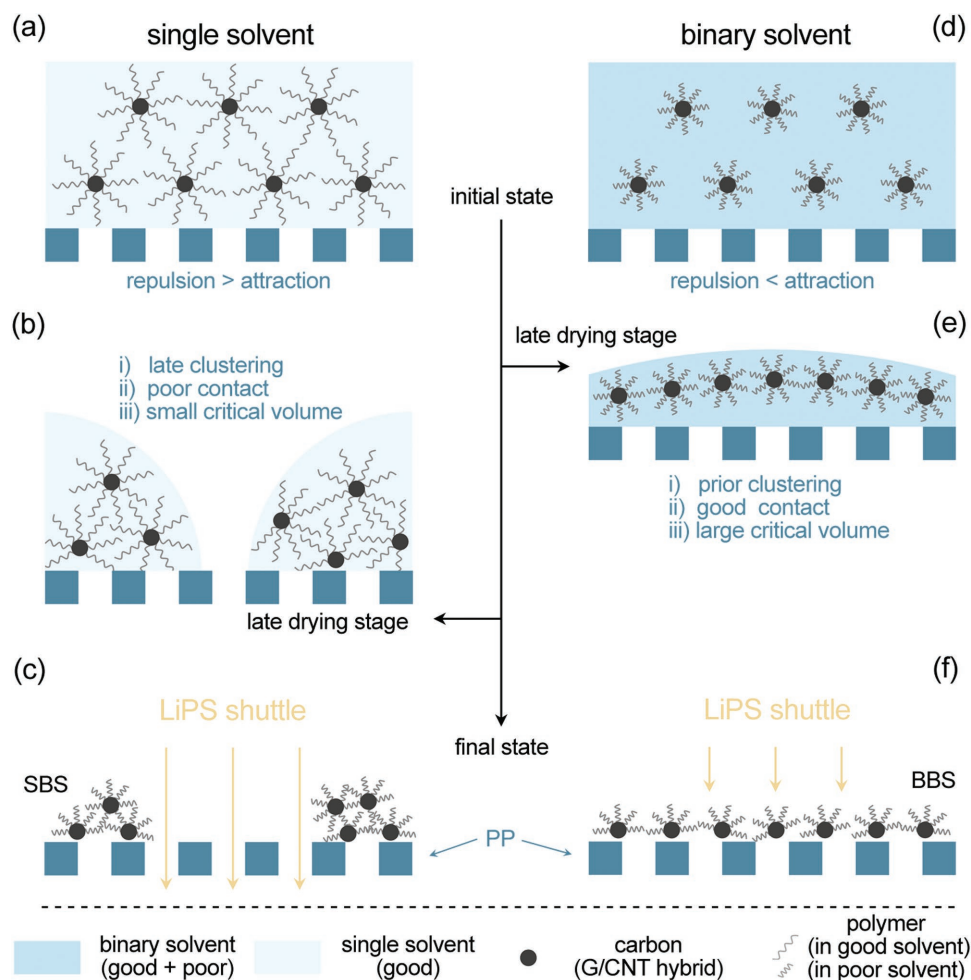


Figure 1. Schematic diagram showing the fabrication process of polysulfide-blocking shields. a) When a single solvent is used, its good solubility of polymer leads to severe interparticle repulsion initially and b) clustering does not occur until the late drying stage. At that time, the critical volume of liquid for precipitation is quite small. Due to the large surface tension, the colloid droplets exhibit poor extensibility. c) Finally, a nonuniform coating of SBS is generated. d) When a binary solvent is used, the solubility of polymer binder and thus the interparticle repulsion is reduced, triggering colloid attraction and clustering prior to the late drying stage. e) At the late drying stage, colloid solution can spread well due to the large critical volume (sufficient amount for forming a liquid film) and small surface tension (for film spreading). f) Finally, a thin and compact coating of BBS is produced, fully hindering the transport of LiPSs.

solvent, the second solvent, as a complementary to water, ideally must hold the following attributes including 1) poorer solubility of PAA, 2) smaller surface tension, and 3) lower vapor pressure (i.e., boiling point) to allow faster drying at a mild temperature (e.g., 60 °C) than water, as well as 4) miscibility with water to prevent undesirable phase separation and achieve homogeneous dispersion/deposition. In addition, this solvent is better to be green and inexpensive so as not to offset the merits of water. According to these requirements, ethanol appears to be an ideal candidate due to its small surface tension (22.10 mN m⁻¹ at 20 °C in air; 72.80 mN m⁻¹ for water) and low boiling point (78.2 °C; 100.0 °C for water). And, the solubility of PAA in ethanol was examined (Figure S3, Supporting Information). Unlike deionized water in which PAA was completely dissolved, ethanol hardly exhibited solubility of PAA and thereby is regarded as a suitable destabilization solvent.

During the preparation of precursor slurry, six seventh of water by volume was replaced by ethanol; while the

concentration of carbon/binder remained the same as 10 g L⁻¹. After blade coating on a porous polypropylene (PP) membrane and drying at 60 °C for 4.0 h, a large piece of modified separator with a uniform coating of BBS (0.3 mg cm⁻²) was obtained (Figure S4, Supporting Information). Separators with a SBS coating were also fabricated using only water as the solvent. The simple modulation of solvent formula shows a profound influence on the morphology of functional layers. Unlike the pristine PP separator with abundant slight macropores (≈100 nm in width and ≈1 μm in length) (Figure S5, Supporting Information), through which LiPSs can easily pass, both SBS and BBS separators exhibit a certain degree of surface coverage by the nanocarbon/PAA composite layer (Figure 2a,b). Nevertheless, the SBS is highly inhomogeneous with many bulges of several micrometers in lateral size. Between these bulges are micrometer-sized holes, exposing the underneath PP substrate (Figure 2c). Thus, LiPS diffusion through these holes is very likely to occur in a working Li-S cell with a SBS separator.

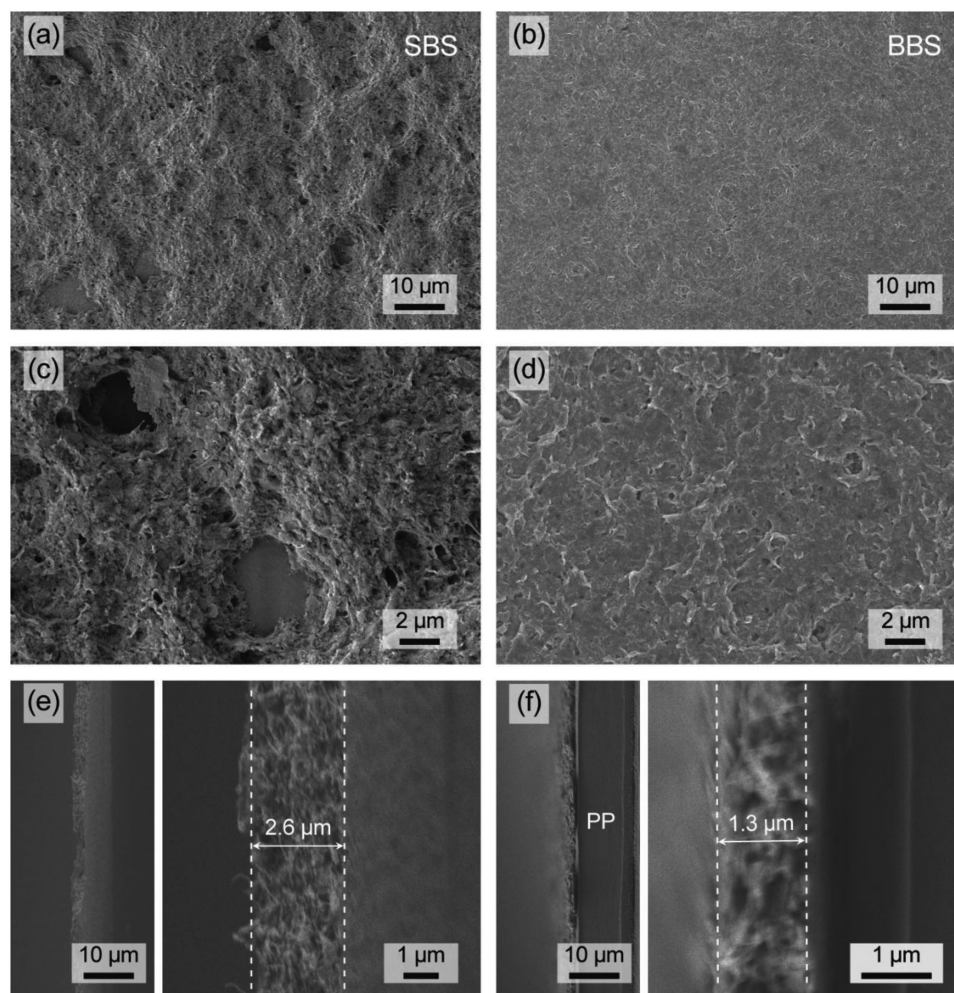


Figure 2. Morphology characterization of BBS and SBS. Top-view SEM images of a,c) SBS and b,d) BBS. Cross-sectional SEM images of e) SBS and f) BBS.

The unique surface morphology of SBS is attributed to the strong surface tension-induced water evaporation, resembling the “coffee ring” effect.^[22] On the contrary, the BBS has a uniform and even surface at almost all regions (Figure 2b). Despite the existence of few surface defects, these defects are concealed by the underneath dense composite framework, not exposing the underlying PP membrane (Figure 2d). The difference in surface morphology exactly resembles the paradigms described in Figure 1.

The solid fraction and the water/ethanol ratio were found to have profound influence on separator structure and properties. Increasing the weight concentration of carbon/binder from 10 to 20 and 30 g L⁻¹, respectively, led to an inhomogeneous morphology of coating layer (Figures S6 and S7, Supporting Information). The high initial volume fraction indicates that colloidal clusters cannot completely diffuse to the liquid/gas interface for assembly within short drying duration. Increasing the volume ratio of water/ethanol from 1:6 to 1:10 resulted in a naturally “stripped” coating (Figure S8a, Supporting Information). Scanning electron microscopy (SEM) image shows that a high percentage of underlying PP substrate is exposed without

BBS protection (Figure S8b, Supporting Information). The BBS ($V_{\text{water}}/V_{\text{ethanol}} = 1:10$) seems to be prone to easy exfoliation from the PP substrate, suggesting the weak adhesion. Such a weak adhesion is likely ascribed to the self-entanglement of PPA chains in a quite poor solvent environment as there are many polymer filaments observed (Figure S8b, Supporting Information). Similar to SBS, the incomplete concealing of underneath throughout pores in these controlled BBS samples obviously will weaken the polysulfide blocking ability. The detailed electrochemical performance will be presented later.

Besides the surface morphology, the solvent engineering also affects the adhesion property and thickness of functional layers. After being scratched severely, the BBS remained a nearly compact surface, but the SBS was almost peeled off (Figure S9, Supporting Information). SEM images show that the peeled-off SBS layer possesses a thickness of $\approx 2.6 \mu\text{m}$ and a fluffy and porous cross-section (Figure 2e). While, the BBS is firmly attached to the PP substrate and the thickness of BBS is reduced by a half to $\approx 1.3 \mu\text{m}$ (Figure 2f). The distinct morphological changes in surface compactness, uniformity, and density are all attributed to the simple engineering of solvent

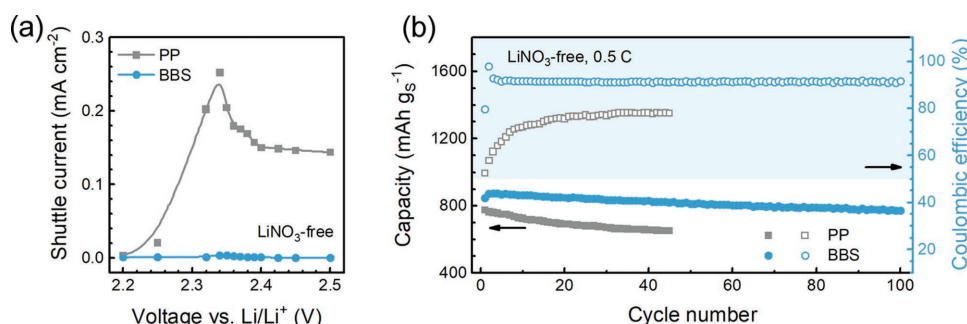


Figure 3. Polysulfide blockage in a LiNO₃-free condition. Comparisons between Li–S cells using a PP and BBS separator, respectively, on a) shuttle current versus applied potentiostatic charging voltage and b) cycling performance at 0.5 C.

from a single one to a rationally designed binary system. The as-obtained BBS holds promising merits of being compact, uniform, thin, and dense, so as to fully exert the abundant interior effective pores of G/CNT hybrids and chemical immobilization effect of hydrophilic PAA while to minimize the expense of increasing unnecessary volume.

The BBS separator was evaluated first in Li–S batteries with a lithium nitrate (LiNO₃)-free electrolyte to validate its polysulfide blocking ability (Figure 3). The cathode consisted of CNT/sulfur composites (90 wt%) and a poly(vinylidene fluoride) (PVDF) binder. The actual sulfur content in a cathode is 63 wt% and the areal sulfur loading is 1.2 mg cm⁻². A previously reported method was employed to directly measure the shuttle current in a working Li–S cell.^[23] It is clearly shown that at various potentiostatic voltages, the cell with a BBS separator exhibited significantly decreased shuttle currents by at least 50 times than the control cell (Figure 3a). The rational solvent-engineering strategy enables more compact and dense coating, as well as smaller shuttle currents, than those reported in our previous works with highly porous architecture.^[12,13] The shuttle inhibition was also implied by the enhanced Coulombic efficiency during cycling at 0.5 C (Figure 3b). The Coulombic efficiency of control cell increased gradually from ~50% to less than 80%; on the contrary, the BBS cell generally displayed a steady Coulombic efficiency of 91–93% since the third cycle.

Despite the polysulfide blocking ability of BBS, LiNO₃ plays a vital role in stabilizing the lithium metal anode for long duration, especially at a high sulfur loading or high current densities. In this regard, 2 wt% LiNO₃ was added in routine 1.0 mol L⁻¹ lithium bis(trifluoromethanesulfonyl) imide-1,3-dioxolane/1,2-dimethoxyethane electrolyte for the following battery tests. At current densities of 0.1, 0.2, 0.5, 1.0, and 2.0 C (1.0 C = 1672 mA g⁻¹, according to the mass of sulfur), the Li–S cell with BBS delivered capacities of 1193, 1008, 888, 800, and 758 mAh g⁻¹, respectively (Figure 4a). In comparison, the control cell with an unmodified PP separator generally obtained ~100 mAh g⁻¹ lower capacities. Especially at a high current density of 2.0 C, the discharge capacity was only ~59% (447 mAh g⁻¹) of the BBS-modified cell. Besides the capacities, the BBS also contributed to reduced voltage polarization at each rate, as typical multiplateau galvanostatic discharge–charge profiles indicated (Figure 4b). Taken at 50% depth of discharge, the polarization voltages for the routine cell with a PP separator and the BBS cell are 259/522 and 187/343 mV at

0.2/2.0 C, respectively (Figure 4c). The largely reduced voltage polarization, along with the extended low voltage plateau corresponding to kinetically sluggish LiPS–Li₂S₂/Li₂S conversion, indicates that the modification of a conductive and LiPS-trapping BBS layer promotes the reaction kinetics significantly. The kinetic promotion by BBS is also evidenced by the sharper and stronger redox peaks in cyclic voltammetric curves (Figure S10, Supporting Information), as well as the smaller charge-transfer impedance in electrochemical impedance spectra (Figure S11, Supporting Information) than the control cell.

Previous studies demonstrated the effectiveness of building a composite interlayer or coating layer to mitigate LiPS shuttle, which, however, mainly focused on the design and combination of component materials. We herein suggest that material processing is of equal importance to fully prove the applicable potential of advanced energy materials. In terms of the cycling performance, the proposed solvent-engineering strategy leaves a noticeable impact on electrochemical performance for SBS and BBS yet composed of the same materials (Figure 4d). In comparison with the control cell with a PP separator, which exhibited an initial capacity of 823 mAh g⁻¹ at 0.5 C and maintained its 56% (461 mAh g⁻¹) after 150 cycles, the SBS-modified cell indicated an enhancement in capacity retention during the initial 100 cycles but finally delivered a comparable capacity of 460 mAh g⁻¹ at the 150th cycle. The initial enhancement, as well as the slightly increased Coulombic efficiency, implies some benefits from SBS, which is yet not sustainable and remarkable. In sharp contrast, the BBS, despite the same composition as the SBS, rendered the Li–S cell with significantly improved cycling performance as ~70% of the initial capacity (860 mAh g⁻¹) was retained after 400 cycles, corresponding to a low cyclic decay rate of 0.078%. Such a distinct difference in the battery cycling stability is ascribed to the different surface morphologies induced by the two rationalized solvent-engineering strategies. The film compactness, the less defects, and the dense structure with minimized ineffective volume of BBS enabled by the binary solvent give rise to better inhibition of LiPS shuttle.

Extra control electrochemical tests validated that materials' selection and processing parameters also strongly affect the cycling performance. A nonaqueous SBS separator synthesized from a PVDF/*N*-methyl-2-pyrrolidinone system demonstrated inferior cycling performance with only 66% of the cell initial capacity retained (Figure S12, Supporting Information).

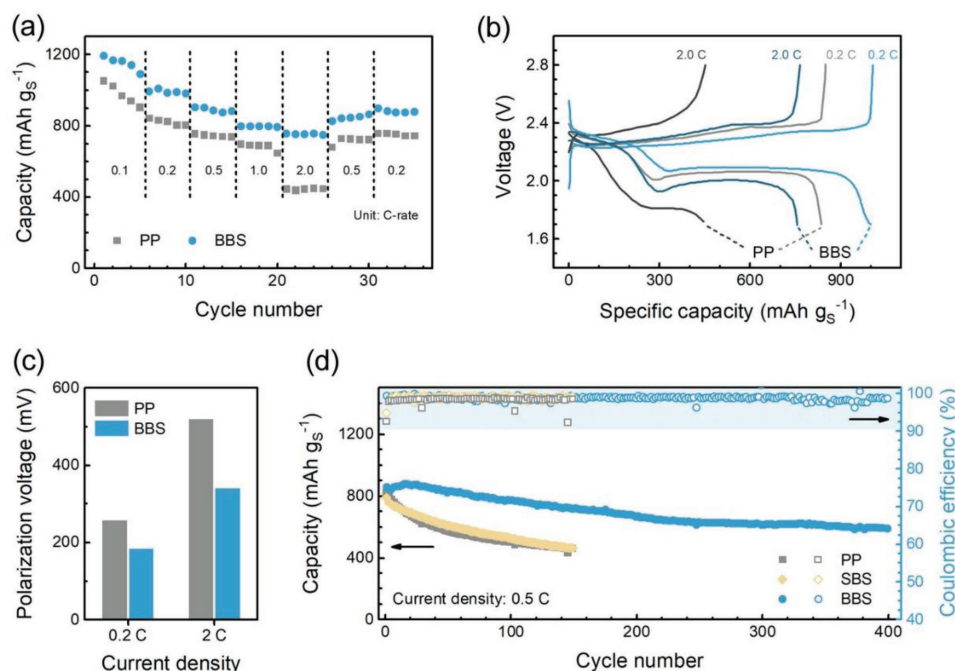


Figure 4. Electrochemical performance of Li-S cells using various separators of PP, BBS, and SBS. a) Rate performance. b) Galvanostatic discharge-charge profiles at 0.2 and 2.0 C, respectively. c) The corresponding polarization voltages. d) Cycling performance at 0.5 C.

The Coulombic efficiency even underwent a drastic drop from around 100% to less than 70%, implying an upcoming cell failure. Therefore, an aqueous binder with good polarity to immobilize polysulfides is critical. Besides, for the PAA/water/ethanol system, the inhomogeneous morphology biased from an ideal BBS, induced by a high ethanol ratio ($V_{\text{water}}/V_{\text{ethanol}} = 1:10$), also weakened the cycling performance despite the same coating composition to ideal BBS (Figure S13, Supporting Information).

The mitigated LiPS shuttle by BBS leads to effective stabilization of both the sulfur cathode and the lithium anode. After 400 cycles at 0.5 C, the sulfur cathode with a BBS well preserved its surface porosity to allow facile electrolyte infiltration and ion transport (Figure 5a). When with the routine PP separator, severe phase migration induced by LiPS diffusion and reprecipitation occurred, leading to a dense and electrolyte-impermeable passivation layer on the top of sulfur cathode (Figure 5b).^[8,24] This passivation layer significantly increased the internal cell resistance, resulting in large polarization and poor reaction reversibility.^[25] Compared to the sulfur cathode, the introduction of BBS had a more profound influence on the lithium anode. There are no cracks or dendrites but a smooth surface observed for the cycled lithium anode protected by a BBS (Figure 5c). On the contrary, the lithium anode cycled with a PP separator suffered from severe corrosion from LiPSs and was pulverized into highly resistive phases mainly consisting of dead lithium surrounded by insulating Li_2S products (Figure 5d). This result again emphasizes the substantially impeded effectiveness of LiNO_3 additive when LiPSs shuttle to the anode and compete with LiNO_3 in anode reactions rampantly and highlights the role of a LiPS-blocking/-scavenging layer with a

good quality to synergistically work with LiNO_3 for efficient electrode stabilization.^[9,12]

Because the concept of functional interlayers/separators is always judged by concerns about its practicality associated with the extra weight and volume, the BBS separator was further evaluated in high-sulfur-loading Li-S cells.^[4] Increasing the sulfur loading contributes to a higher mass/volume fraction of active materials in the whole device and similarly reduces the influence of an interlayer or extra functional layer on the overall mass/volume as well. Thick sulfur cathodes with high sulfur loadings of 3.6 and 7.1 mg cm^{-2} were fabricated, possessing thicknesses of 132 and 193 μm , respectively (Figure S14, Supporting Information). With a sulfur loading of 3.6 mg cm^{-2} , both the cells with a PP or a BBS separator exhibit typical two-plateau galvanostatic discharge profiles at 0.2 C (1.20 mA cm^{-2}), but there is a huge voltage “dip” between the two plateaus for the control PP cell, indicating the large overpotential for $\text{Li}_2\text{S}_2/\text{Li}_2\text{S}$ nucleation (Figure 6a).^[12] For the BBS cell, further increasing the sulfur loading to 7.1 mg cm^{-2} only lowered the discharge capacity and increased voltage polarization slightly, considering the increased current density (0.2 C; 2.37 mA cm^{-2}). As a comparison, the PP cell with a high sulfur loading of 7.1 mg cm^{-2} completely lost the low-plateau feature. Since routine high-sulfur-loading Li-S cells suffer from a severer kinetic issue than low-loading cells due to the longer transport distances for ions/electrons, larger LiPS fluxes across per unit area, thicker passivation layers on both cathode and anode, and the resultant significantly higher internal resistance, this issue was shown to be well addressed by employing a thin, compact, and multifunctional BBS. Along with the enhanced kinetics, BBS also rendered the high-sulfur-loading cells with superior

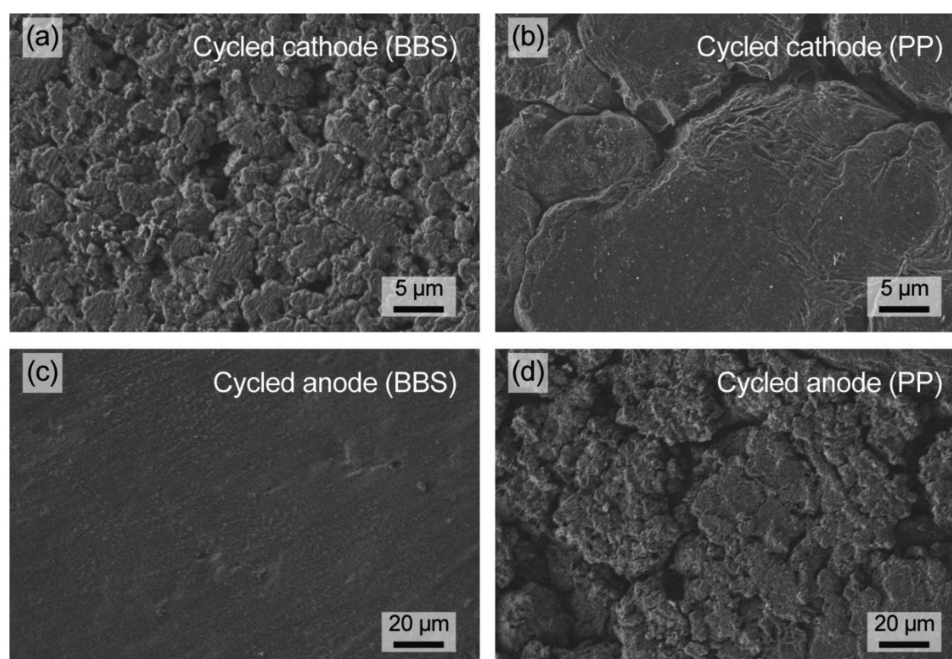


Figure 5. Morphologies of cathodes and anodes in Li-S cells after 400 cycles at 0.5 C, using BBS and PP as the separator, respectively. SEM images of cycled cathodes using a) BBS and b) PP and cycled anodes using c) BBS and d) PP.

cycling performance at 0.2 C, with 83% (2.55 mAh cm^{-2}) and 85% (4.91 mAh cm^{-2}) of initial capacities retained after 100 cycles for the cells with sulfur loadings of 3.6 and 7.1 mg cm^{-2} , respectively (Figure 6b). The routine PP cells,

however, only afforded relatively poor capacity retention of 2.08 and 0.60 mAh cm^{-2} after merely 20 cycles.

To investigate the influence of extra weight/volume the BBS brought to the whole device, specific gravimetric capacities

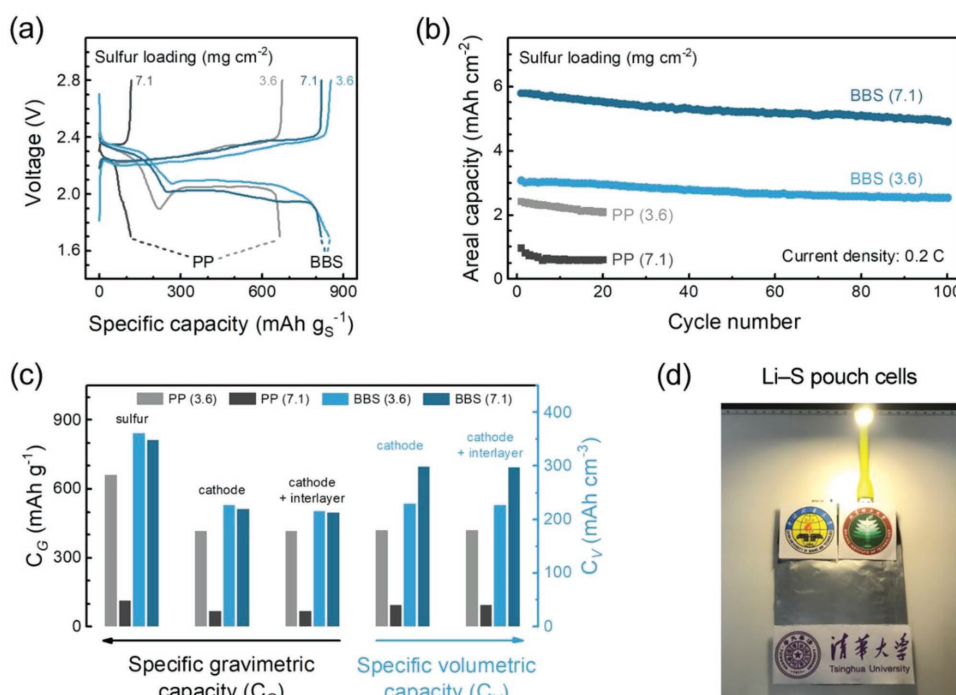


Figure 6. High-sulfur-loading Li-S cells for practical applications. a) Galvanostatic discharge-charge profiles, b) cycling performance, and c) specific gravimetric/volumetric capacities (with respect to the weight of sulfur, cathode, and cathode + interlayer, or the volume of cathode and cathode + interlayer) of Li-S cells with various sulfur loadings (3.6 and 7.1 mg cm^{-2} , respectively) and using different separators (BBS and PP, respectively). d) A practical Li-S pouch cell lighting up a 1.2 W LED.

with respect to the weights of sulfur, cathode, and cathode + interlayer, and specific volumetric capacities with respect to the volumes of cathode and cathode + interlayer are calculated and summarized in Figure 5c. To calculate the volume, the thicknesses of cathodes and interlayers are determined by SEM images. It can be concluded from Figure 5c that: 1) the extra weight/volume has little influence on both capacities, as indicated by comparing the two sets of “cathode” and “cathode + interlayer”; 2) the cell with a higher sulfur loading suffers from smaller impact of the extra weight/volume; 3) even with the extra weight/volume, the actual gravimetric/volumetric capacities of cells with a BBS separator are still higher than those of routine cells. For the BBS cell with the highest sulfur loading of 7.1 mg cm^{-2} , the gravimetric and volumetric capacities based on the weight/volume of cathode + interlayer reached 502 mAh g^{-1} and 299 mAh cm^{-3} , $\approx 590\%$ and $\approx 600\%$ higher than those of a routine PP cell with the same sulfur loading. Besides the high-sulfur-loading coin cells, a practical Li–S pouch cell was assembled to light up a 1.2 W light-emitting diode (LED) for a long time (Figure 6d).

The solvent-engineering strategy presented in this contribution exhibits several remarkable attributes such as 1) simplicity—this strategy only involves the replacement of solvent and conventional slurry coating, requiring no any further time-/energy-consuming steps such as high-energy roll calendaring and no industrially infeasible (e.g., high-volume vacuum filter) or incompatible (e.g., pilot-scale electrostatic spray dryer) infrastructures; 2) versatility—once the basic colloid physical chemistry is well understood for various material–solvent interplays (Figure 1), this strategy can be easily tailored by switching the proof-of-concept water–ethanol binary system to other mixed solvent systems, matching with different functional building blocks (e.g., nonpolar carbon, polar polymer or inorganic materials, and amphiphilic additives) and different substrates with distinct surface polarity (e.g., PP or other polymer separators, glass fiber membranes, ceramic films) to generate tremendous surface functional layers; 3) scalability—this strategy, though being proved in Li–S battery interlayers, can be easily adopted to other components in Li–S batteries and other devices,^[26] such as to the preparation of dense yet porous sulfur cathodes with minimized dead volume that aims at an extremely concerned demand by both academics and industries, that is, lowering the required electrolyte amount and correspondingly improving the cell energy density of Li–S batteries.^[27]

In conclusion, a very simple solvent-engineering strategy by replacing the conventional single-solvent slurry to a binary-solvent slurry was proposed to fabricate large pieces of thin, compact, and multifunctional BBS coating on commercial PP separators through a facile, green, and scalable approach. The BBS consisted of hydrophilic polymer matrix and a highly conductive carbon skeleton to synergistically retard the LiPS shuttle and improve the reaction kinetics of sulfur species. The Li–S batteries with a BBS separator exhibited enhanced rate capability, reduced polarization, superior cycling stability with a low cyclic decay rate of 0.078% for 400 cycles at 0.5 C, and a remarkable capacity of 4.91 mAh cm^{-2} after 100 cycles at 2.37 mA cm^{-2} . The concept of solvent engineering not only renders functional interlayers/separators that significantly improved the Li–S battery performance but also is simple,

versatile, and scalable to be adopted for many other promising research fields of energy storage and materials chemistry. This strategy, in view of material engineering that is usually overlooked, provides an alternative route to explore new materials or optimize the combination of existing materials for the enhancement of actual applications.

Supporting Information

Supporting Information is available from the Wiley Online Library or from the author.

Acknowledgements

J.-L.Q. and H.-J.P. contributed equally to this work. This work was supported by the National Key Research and Development Program (2016YFA0202500 and 2016YFA0200102), the National Natural Science Foundation of China (21776019 and 21676160), and the Young Elite Scientists Sponsorship Program by CAST (2015QNRC001).

Conflict of Interest

The authors declare no conflict of interest.

Keywords

composite electrodes, interlayers, lithium–sulfur batteries, polysulfide intermediates, separators, solvents

Received: March 26, 2018

Published online:

- [1] a) H. J. Peng, J. Q. Huang, Q. Zhang, *Chem. Soc. Rev.* **2017**, 46, 5237; b) J. T. Xu, J. M. Ma, Q. H. Fan, S. J. Guo, S. X. Dou, *Adv. Mater.* **2017**, 29, 1606454.
- [2] a) Y. X. Yin, S. Xin, Y. G. Guo, L. J. Wan, *Angew. Chem., Int. Ed.* **2013**, 52, 13186; b) Z. W. Seh, Y. M. Sun, Q. F. Zhang, Y. Cui, *Chem. Soc. Rev.* **2016**, 45, 5605; c) Q. Pang, X. Liang, C. Y. Kwok, L. F. Nazar, *Nat. Energy* **2016**, 1, 16132.
- [3] a) A. Manthiram, S. H. Chung, C. X. Zu, *Adv. Mater.* **2015**, 27, 1980; b) J. Liang, Z. H. Sun, F. Li, H. M. Cheng, *Energy Storage Mater.* **2016**, 2, 76; c) R. P. Fang, S. Y. Zhao, Z. H. Sun, W. Wang, H. M. Cheng, F. Li, *Adv. Mater.* **2017**, 29, 1606823; d) G. Zhang, Z. W. Zhang, H. J. Peng, J. Q. Huang, Q. Zhang, *Small Methods* **2017**, 1, 1700134; e) J. Zhang, H. Huang, J. Bae, S. H. Chung, W. K. Zhang, A. Manthiram, G. H. Yu, *Small Methods* **2018**, 2, 1700279.
- [4] H. J. Peng, J. Q. Huang, X. B. Cheng, Q. Zhang, *Adv. Energy Mater.* **2017**, 7, 1700260.
- [5] a) J. Q. Huang, Q. Zhang, F. Wei, *Energy Storage Mater.* **2015**, 1, 127; b) Y. Y. Xiang, J. S. Li, J. H. Lei, D. Liu, Z. Z. Xie, D. Y. Qu, K. Li, T. F. Deng, H. L. Tang, *ChemSusChem* **2016**, 9, 3023; c) T. Y. Wang, K. Kretschmer, S. H. Choi, H. Pang, H. G. Xue, G. X. Wang, *Small Methods* **2017**, 1, 1700089; d) Y. C. Jeong, J. H. Kim, S. Nam, C. R. Park, S. J. Yang, *Adv. Funct. Mater.* **2018**, 28, 1707411.
- [6] Y. S. Su, A. Manthiram, *Chem. Commun.* **2012**, 48, 8817.
- [7] a) J. Q. Huang, T. Z. Zhuang, Q. Zhang, H. J. Peng, C. M. Chen, F. Wei, *ACS Nano* **2015**, 9, 3002; b) J. Y. Hwang, H. M. Kim,

- S. K. Lee, J. H. Lee, A. Abouimrane, M. A. Khaleel, I. Belharouak, A. Manthiram, Y. K. Sun, *Adv. Energy Mater.* **2016**, 6, 1501480; c) H. Q. Wang, W. C. Zhang, H. K. Liu, Z. P. Guo, *Angew. Chem., Int. Ed.* **2016**, 55, 3992; d) L. B. Xing, K. Xi, Q. Y. Li, Z. Su, C. Lai, X. S. Zhao, R. V. Kumar, *J. Power Sources* **2016**, 303, 22; e) J. Balach, H. K. Singh, S. Gomoll, T. Jaumann, M. Klose, S. Oswald, M. Richter, J. Eckert, L. Giebeler, *ACS Appl. Mater. Interfaces* **2016**, 8, 14586; f) C. H. Chang, S. H. Chung, A. Manthiram, *Small* **2016**, 12, 174; g) P. Y. Zhai, H. J. Peng, X. B. Cheng, L. Zhu, J. Q. Huang, W. C. Zhu, Q. Zhang, *Energy Storage Mater.* **2017**, 7, 56.
- [8] H. J. Peng, D. W. Wang, J. Q. Huang, X. B. Cheng, Z. Yuan, F. Wei, Q. Zhang, *Adv. Sci.* **2016**, 3, 1500268.
- [9] L. Qie, C. X. Zu, A. Manthiram, *Adv. Energy Mater.* **2016**, 6, 1502459.
- [10] a) S. H. Chung, A. Manthiram, *Adv. Mater.* **2014**, 26, 7352; b) Z. B. Xiao, Z. Yang, L. Wang, H. G. Nie, M. E. Zhong, Q. Q. Lai, X. J. Xu, L. J. Zhang, S. M. Huang, *Adv. Mater.* **2015**, 27, 2891; c) S. Y. Bai, X. Z. Liu, K. Zhu, S. C. Wu, H. S. Zhou, *Nat. Energy* **2016**, 1, 16094; d) C. Y. Fan, H. Y. Yuan, H. H. Li, H. F. Wang, W. L. Li, H. Z. Sun, X. L. Wu, J. P. Zhang, *ACS Appl. Mater. Interfaces* **2016**, 8, 16108; e) M. S. Kim, L. Ma, S. Choudhury, S. S. Moganty, S. Wei, L. A. Archer, *J. Mater. Chem. A* **2016**, 4, 14709; f) W. B. Kong, L. J. Yan, Y. F. Luo, D. T. Wang, K. L. Jiang, Q. Q. Li, S. S. Fan, J. P. Wang, *Adv. Funct. Mater.* **2017**, 27, 1606663; g) T. H. Zhou, W. Lv, J. Li, G. M. Zhou, Y. Zhao, S. X. Fan, B. L. Liu, B. H. Li, F. Y. Kang, Q. H. Yang, *Energy Environ. Sci.* **2017**, 10, 1694.
- [11] J. H. Kim, J. Seo, J. Choi, D. Shin, M. Carter, Y. Jeon, C. W. Wang, L. B. Hu, U. Paik, *ACS Appl. Mater. Interfaces* **2016**, 8, 20092.
- [12] H. J. Peng, Z. W. Zhang, J. Q. Huang, G. Zhang, J. Xie, W. T. Xu, J. L. Shi, X. Chen, X. B. Cheng, Q. Zhang, *Adv. Mater.* **2016**, 28, 9551.
- [13] L. Kong, H. J. Peng, J. Q. Huang, W. C. Zhu, G. Zhang, Z. W. Zhang, P. Y. Zhai, P. P. Sun, J. Xie, Q. Zhang, *Energy Storage Mater.* **2017**, 8, 153.
- [14] W. Liu, J. B. Jiang, K. R. Yang, Y. Y. Mi, P. Kumaravadeivel, Y. R. Zhong, Q. Fan, Z. Weng, Z. S. Wu, J. J. Cha, H. H. Zhou, V. S. Batista, G. W. Brudvig, H. L. Wang, *Proc. Natl. Acad. Sci. USA* **2017**, 114, 3578.
- [15] M. Shaibani, A. Akbari, P. Sheath, C. D. Easton, P. C. Banerjee, K. Konstantas, A. Fakhfour, M. Barghamadi, M. M. Musameh, A. S. Best, T. Ruther, P. J. Mahon, M. R. Hill, A. F. Hollenkamp, M. Majumder, *ACS Nano* **2016**, 10, 7768.
- [16] T. Z. Zhuang, J. Q. Huang, H. J. Peng, L. Y. He, X. B. Cheng, C. M. Chen, Q. Zhang, *Small* **2016**, 12, 381.
- [17] S. Z. Niu, W. Lv, G. M. Zhou, H. F. Shi, X. Y. Qin, C. Zheng, T. H. Zhou, C. Luo, Y. Q. Deng, B. H. Li, F. Y. Kang, Q. H. Yang, *Nano Energy* **2016**, 30, 138.
- [18] M. A. Boles, M. Engel, D. V. Talapin, *Chem. Rev.* **2016**, 116, 11220.
- [19] D. H. Napper, *J. Colloid Interface Sci.* **1977**, 58, 390.
- [20] M. Q. Zhao, H. J. Peng, Q. Zhang, J. Q. Huang, G. L. Tian, C. Tang, L. Hu, H. R. Jiang, H. Y. Cai, H. X. Yuan, F. Wei, *Carbon* **2014**, 67, 554.
- [21] a) M. Q. Zhao, X. F. Liu, Q. Zhang, G. L. Tian, J. Q. Huang, W. C. Zhu, F. Wei, *ACS Nano* **2012**, 6, 10759; b) Z. Zhang, L. L. Kong, S. Liu, G. R. Li, X. P. Gao, *Adv. Energy Mater.* **2017**, 7, 1602543.
- [22] R. D. Deegan, O. Bakajin, T. F. Dupont, G. Huber, S. R. Nagel, T. A. Witten, *Nature* **1997**, 389, 827.
- [23] D. Moy, A. Manivannan, S. R. Narayanan, *J. Electrochem. Soc.* **2015**, 162, A1.
- [24] H. J. Peng, W. T. Xu, L. Zhu, D. W. Wang, J. Q. Huang, X. B. Cheng, Z. Yuan, F. Wei, Q. Zhang, *Adv. Funct. Mater.* **2016**, 26, 6351.
- [25] H. J. Peng, J. Q. Huang, X. Y. Liu, X. B. Cheng, W. T. Xu, C. Z. Zhao, F. Wei, Q. Zhang, *J. Am. Chem. Soc.* **2017**, 139, 8458.
- [26] X. F. Yang, Y. Q. Chen, M. R. Wang, H. Z. Zhang, X. F. Li, H. M. Zhang, *Adv. Funct. Mater.* **2016**, 26, 8427.
- [27] Q. Pang, X. Liang, C. Y. Kwok, J. Kulisch, L. F. Nazar, *Adv. Energy Mater.* **2017**, 7, 1601630.